The parametrically excited upside-down rod: an elastic jointed pendulum model

J. Galán[a],*, W.B. Fraser[b], D.J. Acheson[c], A.R. Champneys[d]

[a] *Dpto. de Matemática Aplicada II, Escuela Superior de Ingenieros, Universidad de Sevilla, Camino de los Descubrimientos s/n, 41092 Sevilla, Spain*
[b] *School of Mathematics and Statistics, The University of Sydney, NSW 2006, Australia*
[c] *Jesus College, Oxford OX1 3DW, UK*
[d] *Department of Engineering Mathematics, University of Bristol, Bristol BS8 1TR, UK*

Abstract

A model is studied which consists of a chain of N identical pendulums coupled by damped elastic joints subject to vertical sinusoidal forcing of its base. Particular attention is paid to the stability of the upright equilibrium configuration with a view to understanding recent experimental results on the stabilization of an unstable stiff column under parametric excitation. It is shown via an appropriate scaling argument how the continuum rod model arises by taking the limit $N \to \infty$.

The effect of the inclusion of bending stiffness is first studied via asymptotics and numerics for the case $N = 1$, showing how the static bifurcation of the pendulum varies with the four dimensionless parameters of the system; damping, bending stiffness and amplitude and frequency of excitation. For the multiple pendulum system, the bifurcation behaviour of the upright position as a function of the same four parameters is studied via numerical methods applied to the linearized equations. The damping term is found to be crucial in destroying many of the resonant instabilities that occur in the limit as $N \to \infty$. At realistic damping levels only a few instabilities remain, which are shown to be largely independent of N. These instabilities agree qualitatively with the experiments.
© 2003 Elsevier Ltd. All rights reserved.

1. Introduction

It is now well known that a simple pendulum can be stabilized in the inverted position by application of a parametric (i.e., vertical) sinusoidal displacement of appropriate (sufficiently

---

*Corresponding author. Tel.: + 34-95-448-6168; fax: + 34-95-448-6165.

E-mail address: jgv@matina.us.es (J. Galán).

high) frequency and (sufficiently small) amplitude [1]. The phenomenon comes about because of the resonance tongue in the 'negative gravity' region of the parameter plane of the classical Mathieu equation. More recently, Acheson [2] (see also the earlier analysis of Otterbein [3]) has shown that the stability of the inverted equilibrium position of a chain of N pendulums can be reduced by modal analysis to the study of N uncoupled Mathieu equations with different parameters. Hence by choosing the frequency sufficiently high and amplitude sufficiently small for each normal mode, the finite chain can also be stabilized by parametric excitation. Numerical simulations for chains of 2 and 3 pendulums [2] and experiments by Acheson and Mullin [4] show that the stability is remarkably robust even for quite large disturbances.

It has been suggested that the limit of this system, in which the total length and mass of the system stays constant while the number of pendulums in the chain becomes infinite, could be used as a possible explanation of the so called 'Indian rope trick' [5]. Unfortunately, as is shown in the afore-mentioned papers, in this limit, which is that of a piece of string, the stability region becomes vanishingly small and the explanation fails.

However, a further experiment by Acheson and Mullin announced in Refs. [6,7], demonstrated that a piece of 'bendy curtain wire', clamped at the bottom and free at the top, that is just too long to support its own weight can be stabilized by parametric oscillation. This might be called the 'Indian rod trick'. Recently, Champneys and Fraser [8] proposed a linearized analysis of the problem for continuously flexible linearly elastic rod. The principle that stabilization is indeed possible was indeed proved using a combination of harmonic balance and double-scale asymptotics, but there remains a lack of qualitative and quantitative fit with the experiments (the details of which appear elsewhere [9]). Part of the problem is that this is an infinite degree-of-freedom system and there are infinitely many resonance tongues within a finite region of parameter space. Nevertheless, a recent extension of this asymptotic analysis [10], which also includes weakly non-linear terms, has shown how the theory of 'resonant tongue interaction' plays a vital role. However, the asymptotic method used breaks down with the inclusion of any small damping in the model, and yet this damping is responsible in practice for destroying all but the finite number of resonant instabilities that are observed in practice.

An alternative approach proposed here is to study a discrete model in which small amounts of damped elastic constraints are added to the bottom joint and the joints between a system of N identical pendulums. By an appropriate scaling, it will be shown that this problem can be posed in such a way as to tend to the materially damped linearly elastic rod in a continuum limit obtained by letting $N \to \infty$. A justification for studying the problem for fixed (large) N is that it can be seen that such material damping enters the model in a regular way, whereas it is a singular perturbation to the continuum problem.

In analyzing such a model, clearly if the stiffness of each joint is high then the state where all pendulums point vertically upwards is stable even in the absence of external forcing. A natural question to ask is therefore "what is the *minimum* amount of elastic stiffness that will just stabilize the parametrically excited inverted chain when the above limit process is applied?" Also, "how does this stability limit depend on the other parameters; damping, and amplitude and frequency of excitation?". This paper addresses these questions using numerical bifurcation theory applied to the equations linearized around the vertical position.

In the next section the fully non-linear system of equations for the N-pendulum configuration is derived and it is shown how this reduces in the limit to the equation for a damped version of the

continuously flexible column investigated by Champneys and Fraser. Section 3 then focuses on the case $N = 1$, treating the non-linear equation, and investigates the effect of the inclusion of bending stiffness by both asymptotic (averaging) and numerical methods. Section 4 then goes on to present the numerical results for general systems of $N > 1$ pendulums. The primary 'leaning over' instability is shown to occur at bending stiffness values that extrapolate to the correct value for the continuum problem. Many other dynamic instabilities are found, but it is shown how damping ameliorates them to the extent that at realistic damping levels only a few remain. Curves of this dynamic, as well as the static instability, are traced out in the remaining three parameters and are shown to be insensitive qualitatively to the value of N provided it is sufficiently large. Finally, Section 5 draws conclusions.

2. The mathematical model

Consider a chain of N simple pendulums, of length ℓ and mass m, linked together in the inverted configuration shown in Fig. 1. Let θ_n be the angle the shaft of the nth pendulum makes with the vertical, and let the lower support point of the system be given the vertical displacement $\Delta \cos \Omega t$. The system is constrained to move in the Oxy-plane with Oy vertically up. Each joint (including the bottom support point) is assumed to have a rotational stiffness k which contributes
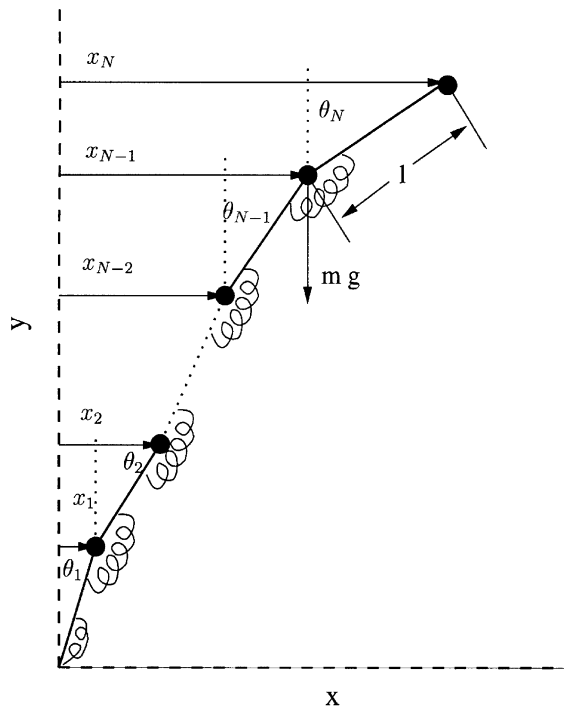

Fig. 1. Model of N identical pendulums. Each pendulum has length l and mass m and there is an elastic spring at each joint. The variable θ_i measures the angle with respect to the previous shaft whereas the generalized co-ordinate x_i measures the horizontal distance to the vertical position of the bob i.

elastic potential energy $k(\theta_n - \theta_{n-1})^2/2$ at the nth joint and $\theta_0 = 0$. That is, each joint is unstressed when each pendulum points vertically. Moreover, each joint is supposed to experience a damping force $\gamma(\dot{\theta}_n - \dot{\theta}_{n-1})$ proportional to the angular velocity of the joint.

2.1. Lagrangian formulation

The Lagrangian for the system can be written in terms of the generalized coordinates θ_n, $n = 1, 2, ..., N$. The Cartesian coordinates of the bob of the nth pendulum are

$$x_n = \sum_{i=1}^{n} \ell \sin \theta_i, \quad y_n = \Delta \cos \Omega t + \sum_{i=1}^{n} \ell \cos \theta_i. \tag{1}$$

Thus, the Lagrangian for this system can be written as

$$\mathscr{L} = \sum_{n=1}^{N} \left\{ \frac{1}{2} m(\dot{x}_n^2 + \dot{y}_n^2) - mgy_n - \frac{1}{2} k(\theta_n - \theta_{n-1})^2 \right\},$$

where in the summation of the last term on the right-hand side $\theta_0 = 0$ and $(\dot{\ }) = \mathrm{d}(\ )/\mathrm{d}t$. The damping is modelled by means of a Rayleigh dissipation function

$$\mathscr{F} = \sum_{n=1}^{N} \frac{\gamma}{2} (\dot{\theta}_n - \dot{\theta}_{n-1})^2.$$

When expressions (1) for the positions x_n, y_n in terms of the generalized co-ordinates θ_n are substituted into the Lagrangian one can then apply Lagrange's equations in the form

$$\frac{\mathrm{d}}{\mathrm{d}t}\left(\frac{\partial \mathscr{L}}{\partial \dot{\theta}_j} \right) - \frac{\partial \mathscr{L}}{\partial \theta_j} + \frac{\partial \mathscr{F}}{\partial \dot{\theta}_j} = 0 \quad \text{for } j = 1, ..., N.$$

Thus, the equation for the jth co-ordinate θ_j is

$$0 = \sum_{n=j}^{N} \left\{ \sum_{i=1}^{n} m[\ell^2 \ddot{\theta}_i \cos(\theta_j - \theta_i) + \ell^2 \dot{\theta}_i^2 \sin(\theta_j - \theta_i)] + [m\ell \Delta\Omega^2 \cos \Omega t - mg\ell] \sin \theta_j \right\}$$
$$- k(\theta_{j+1} - 2\theta_j + \theta_{j-1}) - \gamma(\dot{\theta}_{j+1} - 2\dot{\theta}_j + \dot{\theta}_{j-1})$$

$$= m\ell^2 \left(\cos \theta_j \sum_{n=j}^{N} \sum_{i=1}^{n} [\ddot{\theta}_i \cos \theta_i - \dot{\theta}_i^2 \sin \theta_i] + \sin \theta_j \sum_{n=j}^{N} \sum_{i=1}^{n} [\ddot{\theta}_i \sin \theta_i + \dot{\theta}_i^2 \cos \theta_i] \right)$$
$$+ m(N - j + 1)\ell[\Delta\Omega^2 \cos \Omega t - g] \sin \theta_j - k(\theta_{j+1} - 2\theta_j + \theta_{j-1}) - \gamma(\dot{\theta}_{j+1} - 2\dot{\theta}_j + \dot{\theta}_{j-1}). \tag{2}$$

Note that for $j = 1$ the elastic and the damping term have to be slightly modified.

2.2. Continuum limit

Eqs. (2) will now be linearized on the assumption that $|\theta_n| \ll 1$, $\forall n$, so that $\cos \theta_n \approx 1$, $\sin \theta_n \approx \theta_n$, and the squares and higher powers of small quantities are ignored. The

result is

$$h^2 \sum_{n=j}^{N} \left(\sum_{i=1}^{n} \ddot{\theta}_i \right) + h(N-j+1)(\varepsilon\omega^2 \cos \omega\tau - 1)\theta_j$$

$$- B(\theta_{j+1} - 2\theta_j + \theta_{j-1})/h^2 = \Gamma(\dot{\theta}_{j+1} - 2\dot{\theta}_j + \dot{\theta}_{j-1})/h^2, \tag{3}$$

where the following dimensionless quantities have been introduced, based on the total length and mass of the system $L = N\ell$, $M = Nm$:

$$h = \frac{\ell}{L} = \frac{1}{N}, \quad \varepsilon = \frac{\Delta}{L}, \quad \omega = \frac{\Omega}{\sqrt{g/L}}, \quad \tau = \frac{t}{\sqrt{L/g}},$$

$$B = \frac{k}{MgLN}, \quad \Gamma = \frac{\gamma}{MgLN} \sqrt{\frac{g}{L}},$$

and henceforth $(\dot{\ }) = \partial(\ )/\partial\tau$.

In order to find the continuum column limit of the model described above, first set $jh = s$, $nh = \eta$, $ih = \xi$, and $\theta_n = \phi(s,t)$, $\theta_i = \phi(\xi,t)$, and then take the limit of the above linearized form of the jth Lagrange equation, as $h \to 0$, $N \to \infty$ while L, M, B and Γ are held fixed. Note that both k and γ must therefore scale with N. The result is

$$\int_s^1 \left(\int_0^\eta \ddot{\phi}(\xi,t)\mathrm{d}\xi \right)\mathrm{d}\eta + (\varepsilon\omega^2 \cos \omega\tau - 1)(1-s)\phi(s,\tau) - B\frac{\partial^2 \phi}{\partial s^2} = \Gamma\frac{\partial^2 \dot{\phi}}{\partial s^2}.$$

Finally, differentiation of this result twice with respect to s gives

$$-\ddot{\phi} + (\varepsilon\omega^2 \cos \omega\tau - 1)[(1-s)\phi]'' - B\phi^{\mathrm{IV}} = \Gamma\dot{\phi}^{\mathrm{IV}}, \tag{4}$$

where $(\ )' = \partial(\ )/\partial s$.

This equation is equivalent to that of a continuously flexible column with bending stiffness B and a material damping coefficient Γ. The equivalence of Eq. (4) to Eqs. (3.3)–(3.5) in Ref. [8] can be seen by making the substitutions $\mathbf{r}' = \mathbf{i} \sin \phi \approx \mathbf{i}\phi$ for $|\phi| \ll 1$ and $\Gamma = 0$.

For the majority of the rest of this paper the linearized equation (3) shall be studied. This represents a convenient discretised formulation, because its parameters B, ω, ε and Γ are scaled in such a way that they correspond to those of the continuum model. Also in Ref. [10] it is shown that non-linear terms are not at all crucial in studying how the various instabilities of the vertical equilibrium interact upon varying B, ε and Ω for the continuum model. Hence it would seem reasonable to treat the linearized model (3) which has the huge advantage over (2) that constant matrices, rather than non-linear functions of θ_i, multiply the highest order derivatives. However it is clear that in any practical demonstration of the 'Indian rod trick' damping is important, and Eq. (3) has the advantage over the continuum model (4) in that damping does not enter as a singular perturbation.

Before proceeding, it will be helpful to put Eq. (3) in a more convenient form.

2.3. Writing as a first order system

The linearized form of the Lagrange equations given in Eq. (3) can be written in matrix form as follows (cf. Otterbein [3] who considers the case without stiffness or damping):

$$\mathbf{M}\ddot{\boldsymbol{\Theta}} + (\varepsilon\omega^2\cos\omega\tau - 1)N\mathbf{K}\boldsymbol{\Theta} + BN^4\mathbf{E}\boldsymbol{\Theta} = -\Gamma N^4\mathbf{E}\dot{\boldsymbol{\Theta}}, \tag{5}$$

where

$$\boldsymbol{\Theta} = (\theta_1, \theta_2, \theta_3, \ldots, \theta_N)^{\mathrm{T}},$$

$$\mathbf{M} = \begin{bmatrix} N & N-1 & N-2 & N-3 & \cdots & 1 \\ N-1 & N-1 & N-2 & N-3 & \cdots & 1 \\ N-2 & N-2 & N-2 & N-3 & \cdots & 1 \\ N-3 & N-3 & N-3 & N-3 & \cdots & 1 \\ \vdots & \vdots & \vdots & \vdots & & \vdots \\ 1 & 1 & 1 & 1 & \cdots & 1 \end{bmatrix},$$

$$\mathbf{K} = \begin{bmatrix} N & 0 & 0 & 0 & \cdots & 0 \\ 0 & N-1 & 0 & 0 & \cdots & 0 \\ 0 & 0 & N-2 & 0 & \cdots & 0 \\ 0 & 0 & 0 & N-3 & \cdots & 0 \\ \vdots & \vdots & \vdots & \vdots & & \vdots \\ 0 & 0 & 0 & 0 & \cdots & 1 \end{bmatrix},$$

$$\mathbf{E} = \begin{bmatrix} 2 & -1 & 0 & 0 & \cdots & 0 \\ -1 & 2 & -1 & 0 & \cdots & 0 \\ 0 & -1 & 2 & -1 & \cdots & 0 \\ \vdots & \vdots & \vdots & -1 & 2 & -1 \\ 0 & 0 & 0 & 0 & -1 & 1 \end{bmatrix}.$$

In general then, matrix $\mathbf{M}$ must be inverted in order to write Eq. (5) in first order form. A simpler, physically motivated approach is to introduce the generalized coordinates; $\mathbf{x} = (x_1, x_2, x_3, \ldots, x_N)^{\mathrm{T}}$, via the transformation

$$h\boldsymbol{\Theta} = \mathbf{Tx},$$

where

$$\mathbf{T} = \begin{bmatrix} 1 & 0 & 0 & 0 & \cdots & 0 \\ -1 & 1 & 0 & 0 & \cdots & 0 \\ 0 & -1 & 1 & 0 & \cdots & 0 \\ 0 & 0 & -1 & 1 & \cdots & 0 \\ \vdots & \vdots & \vdots & \vdots & & \vdots \\ 0 & 0 & 0 & 0 & -1 & 1 \end{bmatrix}.$$

The generalized coordinates **x** represent the horizontal displacements of the bobs as depicted in Fig. 1. Thus, in terms of **x**, the matrix form of the linearized Lagrange equations is

$$\ddot{\mathbf{x}} + (\varepsilon\omega^2\cos\omega\tau - 1)N\hat{\mathbf{K}}\mathbf{x} + BN^4\hat{\mathbf{E}}\mathbf{x} = -\Gamma N^4\hat{\mathbf{E}}\dot{\mathbf{x}}, \qquad (6)$$

where $\mathbf{T}^\mathrm{T}\mathbf{M}\mathbf{T} = \mathbf{I}$, $\hat{\mathbf{K}} = \mathbf{T}^\mathrm{T}\mathbf{K}\mathbf{T}$, and $\hat{\mathbf{E}} = \mathbf{T}^\mathrm{T}\mathbf{E}\mathbf{T}$.

In this representation, although the coefficient of $\ddot{\mathbf{x}}$ is greatly simplified, the expressions for $\hat{\mathbf{K}}$ and $\hat{\mathbf{E}}$ are more complicated:

$$\hat{\mathbf{K}} = \begin{bmatrix} 2N-1 & -N+1 & 0 & 0 & 0 & 0 & \cdots & 0 \\ -N+1 & 2N-3 & -N+2 & 0 & 0 & 0 & \cdots & 0 \\ 0 & -N+2 & 2N-5 & -N+3 & 0 & 0 & \cdots & 0 \\ \vdots & \vdots & \vdots & \vdots & \vdots & \vdots & & \vdots \\ 0 & 0 & 0 & 0 & -3 & 5 & -2 & 0 \\ 0 & 0 & 0 & 0 & 0 & -2 & 3 & -1 \\ 0 & 0 & 0 & 0 & 0 & 0 & -1 & 1 \end{bmatrix},$$

$$\hat{\mathbf{E}} = \begin{bmatrix} 6 & -4 & 1 & 0 & 0 & 0 & 0 & 0 & \cdots & 0 \\ -4 & 6 & -4 & 1 & 0 & 0 & 0 & 0 & \cdots & 0 \\ 1 & -4 & 6 & -4 & 1 & 0 & 0 & 0 & \cdots & 0 \\ 0 & 1 & -4 & 6 & -4 & 1 & 0 & 0 & \cdots & 0 \\ 0 & 0 & 1 & -4 & 6 & -4 & 1 & 0 & \cdots & 0 \\ \vdots & \vdots & \vdots & \vdots & \vdots & \vdots & \vdots & \vdots & & \vdots \\ 0 & 0 & 0 & 0 & 0 & 1 & -4 & 6 & -4 & 1 \\ 0 & 0 & 0 & 0 & 0 & 0 & 1 & -4 & 5 & -2 \\ 0 & 0 & 0 & 0 & 0 & 0 & 0 & 1 & -2 & 1 \end{bmatrix}.$$

Unfortunately, it is not possible to uncouple these equations as is the case when $B = \Gamma = 0$, and so one cannot appeal directly to the theory of Mathieu equations as in Ref. [2].

3. Single pendulum with elastic support and damping

Before proceeding to an analysis of the N-pendulum case, it is instructive to carry out an investigation of the simplest approximation to the parametrically excited continuous column; i.e, one pendulum with elastic support and damping. Owing to the simplicity of the model, one can in this case carry out a fully non-linear study, using both averaging theory and numerical bifurcation analysis.

To obtain the single pendulum equation, set $N = 1$, $\theta_1 = \theta$ and $\ell = L$ (so that $h = 1$) in Eq. (2), and introduce the dimensionless variables to find

$$\ddot{\theta} + (\varepsilon\omega^2\cos\omega\tau - 1)\sin\theta + B\theta + \Gamma\dot{\theta} = 0. \qquad (7)$$

Note that the choice of origin of θ is such that the trivial solution $\theta = \dot{\theta} = \ddot{\theta} = 0$ of Eq. (7), for any values of the parameters, corresponds to the inverted pendulum position. The usual down-hanging position is given by $\theta = \pi$. Now to analyze the stability and bifurcation behaviour of the $\theta = 0$ solution.

The case without the elastic joint, i.e., setting coefficient $B = 0$, is well known and can be found in many textbooks [11–13]. See Ref. [14] for some of the most recent results. The bifurcation diagram can be presented either in a dimensionless amplitude–frequency diagram [2], or, if another non-dimensionalization is chosen, in the more familiar Mathieu-like amplitude–gravity diagram with the classical resonance tongues. In fact, the stability of the inverted pendulum solution is given by the linearization of Eq. (7), which leads to the classical damped Mathieu equation;

$$\ddot{\theta} + (\varepsilon\omega^2 \cos \omega\tau - 1 + B)\theta + \Gamma\dot{\theta} = 0. \tag{8}$$

Note that the effect of the stiffness B in this linearized equation is simply to modify the usual gravitational term. However, it is not evident what the effect of the elastic and damping terms are on the fully non-linear Eq. (7).

3.1. Static stability

When $\varepsilon = 0$, the equilibria of Eq. (7) are the solutions of

$$\sin \theta = B\theta.$$

From an analysis of solutions to this equation, it is found that the trivial solution undergoes a supercritical pitchfork bifurcation upon decreasing B through 1. Analyzing the stability of the equilibria using Eq. (8), one finds that the trivial solution is stable for $B > 1$ and the bifurcated ones stable for $B < 1$. Hence, this corresponds to a stable stiff-jointed single pendulum becoming unstable and 'leaning over' to one side as the bending stiffness in the joint is reduced through the critical value, 1 in dimensionless units.

3.2. High-frequency asymptotic limit

The author's now wish to assess what happens to the symmetry-breaking bifurcation when the parametric excitation is added ($\varepsilon > 0$ in Eq. (7)). It is convenient to use the theory of averaging in the limit that the frequency of excitation ω is large.

It is assumed that the time dependence of $\theta(t)$ can be decomposed into a sum of two terms:

$$\theta(t) = \alpha(t) + \xi(t), \tag{9}$$

such that $\langle \theta(t) \rangle = \alpha(t)$ is a function of $O(1)$ that is slowly varying compared with the external forcing, and $\xi(t)$ is a rapidly varying function with small amplitude and zero average over one forcing period. In particular this analysis is valid when $\varepsilon \ll 1$ and $\varepsilon^2\omega^2 \sim O(1)$. Here, the averaging operation over one period of the external force is defined by

$$\langle \Psi \rangle = \frac{\omega}{2\pi} \int_0^{\frac{2\pi}{\omega}} \Psi \, d\tau. \tag{10}$$

Note that the above considerations can be formalized by introducing two time scales t, and $\hat{t} = \varepsilon t$ and letting $\hat{\omega} = \omega\varepsilon = O(1)$. The results from such a formalism (cf. for example the general theory in Ref. [15]) is identical to that obtained below.

Substitution of Eq. (9) into Eq. (7) gives

$$\ddot{\alpha} + \ddot{\xi} + B(\alpha + \xi) + \Gamma(\dot{\alpha} + \dot{\xi}) + (\varepsilon\omega^2 \cos\omega t - 1)(\sin\alpha\cos\xi + \cos\alpha\sin\xi) = 0. \qquad (11)$$

Since ξ is small, take $\cos\xi \sim 1$ and $\sin\xi \sim \xi$ so that the last term becomes

$$(\varepsilon\omega^2 \cos\omega t - 1)(\sin\alpha + \xi\cos\alpha) + O(\xi^2).$$

When this equation is averaged over one period of the fast frequency and the averages $\langle\cos\omega t\rangle = \langle\xi\rangle = \langle\dot{\xi}\rangle = \langle\ddot{\xi}\rangle = 0$ are taken into account, one obtains

$$\ddot{\alpha} + B\alpha + \Gamma\dot{\alpha} - \sin\alpha + \varepsilon\omega^2\cos\alpha\langle\xi\cos\omega t\rangle = 0. \qquad (12)$$

An expression for the term $\langle\xi\cos\omega t\rangle$, is found as follows: First, subtract Eq. (12) from Eq. (11) which gives

$$\ddot{\xi} + B\xi + \Gamma\dot{\xi} + \varepsilon\omega^2\sin\alpha\cos\omega t + \varepsilon\omega^2\cos\alpha(\xi\cos\omega t - \langle\xi\cos\omega t\rangle) = 0. \qquad (13)$$

The dominant term in this equation is $\varepsilon\omega^2\sin\alpha\cos\omega t$, so that an approximate equation for ξ is

$$\ddot{\xi} \simeq -\varepsilon\omega^2\sin\alpha\cos\omega t$$

(note that for consistency $\xi = O(\varepsilon)$ and $\ddot{\xi} = O(\varepsilon^{-1})$ are required, so that the term proportional to Γ in Eq. (13) has been correctly neglected). Integrating twice with respect to time and noting that α is constant over the averaging period with respect to the fast time scale $1/\omega$, gives the result that

$$\xi(t) \simeq \varepsilon\sin\alpha\cos\omega t.$$

This last expression is now used to find

$$\langle\xi\cos\omega t\rangle = \varepsilon\sin\alpha\langle\cos^2\omega t\rangle = \tfrac{1}{2}\varepsilon\sin\alpha. \qquad (14)$$

Substitution of Eq. (14) into Eq. (12) gives the equation that determines the time evolution of the slowly varying component of $\theta(t)$:

$$\ddot{\alpha} + B\alpha + \Gamma\dot{\alpha} + \left(\frac{\varepsilon^2\omega^2}{2}\cos\alpha - 1\right)\sin\alpha = 0. \qquad (15)$$

If $B = 0$, the well-known stability result for the simple pendulum in the high-frequency limit is recovered; if $\varepsilon\omega < \sqrt{2}$ the $\alpha = 0$ solution is unstable, whereas if $\varepsilon\omega > \sqrt{2}$ it is stable. Hence the maximum α which will not result in the pendulum falling over is $\alpha_{max} = \cos^{-1}(2/\varepsilon^2\omega^2)$.

For non-zero B the $\alpha = 0$ solution is stable if $B + \varepsilon^2\omega^2/2 > 1$. Thinking of B as the bifurcation parameter, this gives the correction to the supercritical pitchfork bifurcation found above for the $\varepsilon = 0$ problem, namely that a pendulum with $B > 1 - \varepsilon^2\omega^2/2$ is stable in the upright position. So the effect of parametric forcing in this asymptotic limit is to reduce the B-value that leads to stability. Note that from the point of view of dynamical systems theory, the trivial solution is now a periodic solution and the pitchfork is a symmetry-breaking bifurcation of this periodic solution.

However, equivalently $\varepsilon\omega$ may be thought of as the bifurcation parameter, then it is possible to find that the stability of the bifurcating solutions for B just less than 1 is very different from that for the non-elastic pendulum $B = 0$. In the former case, decreasing $\varepsilon\omega$ leads to an unstable equilibrium surrounded by two stable equilibria, whereas for $B = 0$, there is a *subcritical* pitchfork bifurcation (increasing $\varepsilon\omega$ through $\sqrt{2}$ a stable equilibrium surrounded by two unstable ones is found). Hence for B between 0 and 1 there must be a codimension-two point that accounts for the change between a super- and subcritical pitchfork.

To consider what happens, now focus on the symmetry broken solutions that originate at the pitchfork bifurcation. They are characterized by non-zero equilibria of the averaged Eq. (15), i.e., solutions of

$$B = \left(1 - \frac{\varepsilon^2\omega^2}{2}\cos\alpha\right)\frac{\sin\alpha}{\alpha}. \tag{16}$$

The nature of the bifurcation can be inferred by Taylor expansion in α of the trigonometric functions in Eq. (16):

$$B = 1 - \frac{\varepsilon^2\omega^2}{2} + \left(\varepsilon^2\omega^2 - \frac{1}{2}\right)\frac{\alpha^2}{3}. \tag{17}$$

The solution without external forcing ($\varepsilon = 0$) is stable for $B > 1$ and unstable for $B < 1$. From Eq. (17) it is clear that the bifurcation will be supercritical if $\varepsilon^2\omega^2 - \frac{1}{2} < 0$ (Fig. 2a) and subcritical if $\varepsilon^2\omega^2 - \frac{1}{2} > 0$ (Fig. 2b). Therefore, there is a degenerate pitchfork bifurcation at

$$\varepsilon\omega = \frac{1}{\sqrt{2}}$$

in the high-frequency limit. Emanating from the super-subcritical transition in the (B,ω)-plane there will also be a curve of folds (limit points of branches of the non-trivial periodic solutions), as depicted in Fig. 2b. From the averaging results, the position of the limit points can be estimated from the zeros of $dB/d\alpha$, which, according to the quadratic approximation (17) occur at
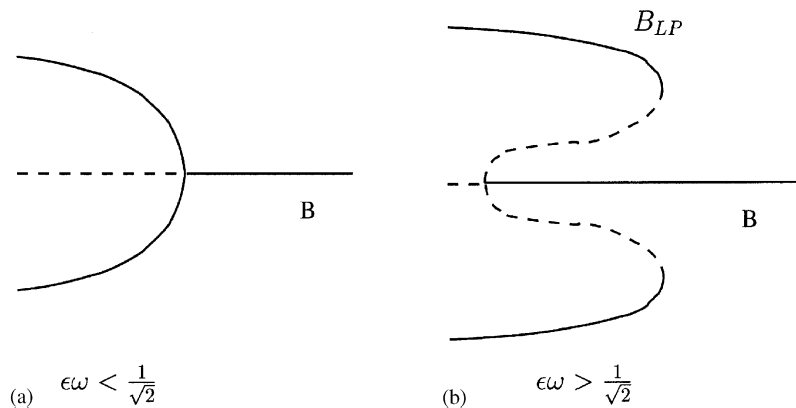

Fig. 2. Schematic bifurcation diagram for a single pendulum. A measure of the amplitude of the solution is plotted as a function of B for fixed value of ε and ω. Panel (a) correspond to a supercritical bifurcation ($\varepsilon\omega < \frac{1}{\sqrt{2}}$) and panel (b) to a subcritical one ($\varepsilon\omega > \frac{1}{\sqrt{2}}$). The turning point ($B_{LP}$) in the subcritical case is approximately given by Eq. (18).

$\alpha = \pm \sqrt{4 - 2/\varepsilon^2\omega^2}$. Substituting this expression for α back into Eq. (17) gives the quadratic approximation to the locus of limit points

$$B_{LP} = \frac{(1 + \varepsilon^2\omega^2)^2}{6\varepsilon^2\omega^2}, \quad \text{for } \varepsilon\omega > \frac{1}{\sqrt{2}}. \tag{18}$$

3.3. Numerical results

Fig. 3 compares the above results from the averaging method with the results of a numerical bifurcation analysis using the numerical continuation code AUTO [16]. Fig. 3a shows an $\varepsilon - \omega$ bifurcation diagram for $B = 0$ and $\Gamma = 0.1$. For small values of ω and ε the pendulum is unstable, but it can be stabilized for certain values inside the shaded region. The borders of the stability region are formed by pitchfork and period-doubling bifurcations, which correspond to harmonic and subharmonic instabilities, respectively. The label ε_1 marks the threshold of stability for the amplitude for a given value of the frequency ω_1 ($\omega_1 = 35.4$, $\varepsilon_1 = 0.04$).

Fig. 3b depicts the position of the pitchfork bifurcation in the $(\omega - B)$-plane for this particular value of $\varepsilon = \varepsilon_1$. Note that the curve should connect the point $(B = 1, \omega = 0)$ with $(B = 0, \omega = \omega_1)$. There is transition from supercritical to subcritical pitchfork bifurcation at the precise value $\omega = 17.71$. Note that this compares very well with the theoretical value $\omega = 1/\varepsilon\sqrt{2} \approx 17.68$ found above analytically in the high-frequency limit, although the value of ε used is just $\frac{1}{25}$. Emanating from the degenerate pitchfork bifurcation point, three curves are shown. The grey line is the approximate position of the limit point for the unstable periodic orbit born at the subcritical pitchfork bifurcation as given by Eq. (18). The solid thick line is the same quantity but derived
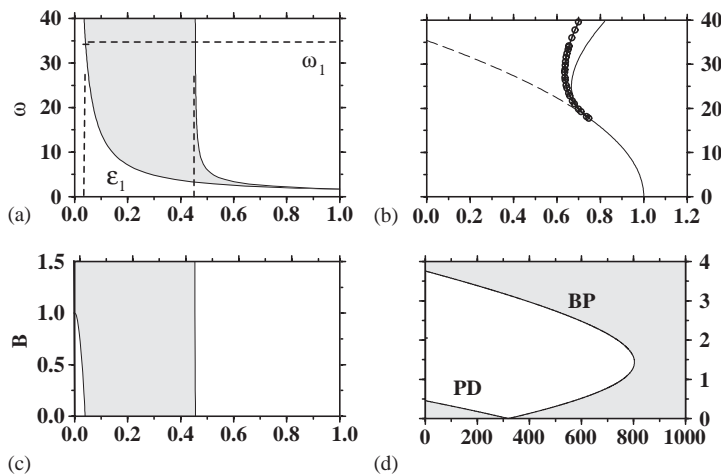

Fig. 3. Bifurcation diagrams for the single pendulum. Panel (a) is the ε–ω bifurcation diagram for $B = 0$ and $\Gamma = 0.1$. Panel (b) is the position of the pitchfork bifurcation in the ω–B plane for a fixed value of ε. We have chosen $\varepsilon = 0.04$ and marked it in panel (a) with the symbol ε_1 and the corresponding frequency with ω_1. See text for explanation of the curves emanating from the codimension-two point. Panel (c) shows the ε–B bifurcation diagram for a fixed value of the frequency, marked by ω_1 in panel (a). The shaded region corresponds to stability of the inverted pendulum position. Panel (d) plots the (ε, B)-bifurcation diagram corresponding to the same values as those used in (c) but in a broader range.

from the full non-linear Eq. (16). Finally, the circles are the numerically computed positions of the limit points from the continuation scheme. The agreement with the prediction of averaging theory is remarkable.

Fig. 3c shows the ε–B bifurcation diagram for a fixed value of the frequency, marked by w_1 in panel (a). The shaded region corresponds to stability of the inverted pendulum position. Fig. 3d is a plot of the same ε–B bifurcation diagram on a much broader range (up to B values corresponding to highly stiff support which is way beyond the region of interest for the primary investigation of this paper). Note that, as argued above, the linearized stability diagram is essentially the same as that of the Mathieu equation with εB playing the role of the frequency parameter. However, as can be seen by running numerical simulations, the non-linear behaviour is entirely different to that of the parametrically excited ($B = 0$) simple pendulum.

A simple QuickBasic program has been written to perform simulations of a single stiff damped parametrically excited pendulum and plot the results in physical configuration space.[1] The results of running this program are striking. For example, setting $\varepsilon = 0.1$, $\omega = 10$, $\Gamma = 0.1$ and allowing B to increase from say 0.25 to 25 will result in a bent-over equilibrium position approaching a stable upside-down configuration for B about 0.64. So a small amount of bending stiffness has a stabilizing influence. In agreement with the above analysis (since $\varepsilon\omega > 1/\sqrt{2}$) there is evidence of hysteresis in that upon decreasing B, the upright equilibrium stays stable until a B-value of approximately 0.5. Now, upon increase of B to 25 the upside down state becomes *unstable* again and large oscillations result. Hence, counterintuitively, making the support much stiffer, has resulted in instability! Further increases of B result in hitting the next stability tongue of Fig. 3d and stability is once again restored. Note that although there is a close analogy with the usual, rigid, unsupported pendulum at the linear level, the non-linear dynamics of the two problems seem very different; compare numerical experiments using the QuickBasic program with those at the corresponding parameter set for the standard parametrically excited pendulum [14].

The situation for N-pendulums is, however, much more complicated. Since there are N normal modes, there will be many other instability tongues around, and depending on the values of the other parameters, these may well not all be bounded away from a small neighbourhood of $B = 1$.

4. Stability of the trivial solution for N pendulums

This section investigates the stability of the trivial solution ($\theta_i = \dot{\theta}_i = 0$ $i = 1, \ldots, N$), of Eq. (5), as the parameters and the number of pendulums are varied. The aim is to gain some insight into the continuum limit (Eq. (4)) and, in particular, explain the experimental stabilization of a flexible and damped curtain wire [9].

4.1. Numerical method

To investigate the stability of the upright solution of the linearized system Eq. (6) use of AUTO has been made in the following way. The starting point is the upright vertical solution (i.e., $x_i = 0$) for a fixed number of pendulums. This is represented as a periodic solution of the

---

[1]The interested reader can find the details and download the program via the web page www.jesus.ox.ac.uk/~dacheson.

non-autonomous system of ODEs. Then continue this solution, which is trivial, as one of the parameters (B, ε, ω or Γ) varies. In so-doing it is possible to monitor the characteristic (Floquet) multipliers and accurately locate bifurcation points, at which multipliers cross the unit circle. In order to extract information on the continuous limit, follow a straightforward scaling analysis by plotting the relevant quantities as a function of $1/N$ and extrapolating the result to the origin.

Once a bifurcation point is located, it is possible to continue it in two parameters and determine the stability regions of the system. Alternatively, investigations into the spatial and temporal character of the mode that is bifurcating can be performed by demanding that AUTO switches branches at the bifurcation point. Since one is using the linearized equations, this will compute a pure 'vertical branch' of solutions at fixed parameter values, which can be plotted at a fixed non-zero value of the solution's norm. However, one cannot detect non-linear behaviour such as the super or subcriticality of the bifurcation or any secondary bifurcations since the linearized equations have been used.

4.2. Static instability

In the absence of external forcing ($\varepsilon = 0$) and elastic restoring forces ($B = 0$) the system of N pendulums (and its continuous counterpart) is unstable in its upright position ($x_i = 0$, $i = 1, \ldots, N$). As the elastic term is increased, this solution becomes stable. For the continuous system, the critical value of B for this transition in dimensionless values is $B_{cr} = 0.127594$ (see Refs. [8,17] for how this number is determined exactly in terms of the first zero of a certain Bessel function). In Fig. 4a is plotted the critical values of $B_{cr}^{(N)}$ as a function of the number of pendulums for $\varepsilon = 0$. In
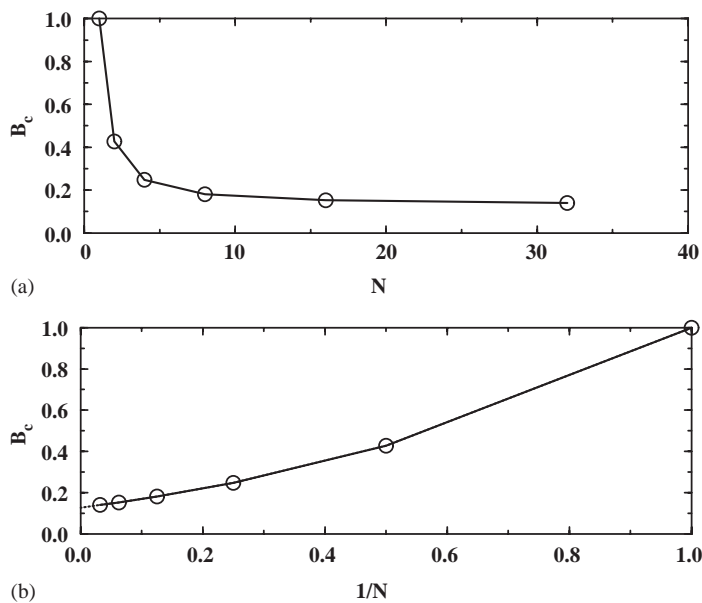

Fig. 4. The upper part of the figure shows the critical values of B as a function of the number of pendulums N. They approach the value corresponding to the continuum limit ($B_\infty = 0.1278$) in an asymptotic way. The lower figure shows the same quantity as a function of $1/N$ to make the scaling behaviour more evident. The dashed line is the quadratic extrapolation to the origin that gives an estimation of $B = 0.1275$ for the critical value of the elastic coefficient.

the previous section it has already been seen that $B_{cr}^{(1)} = 1$. These results now show that $B_{cr}^{(N)}$ decreases monotonically from this value as N increases. To extrapolate to the value as $N \to \infty$ the same values as a function of $1/N$ have been plotted in Fig. 4b. A quadratic fit of the points evaluated at $1/N = 0$ indicates that the estimation of the critical value as the number of pendulums goes to infinity is $B_\infty = 0.1278$, in very good agreement with the continuum value.

4.3. The effect of damping

In the continuous model the undamped ($\Gamma = 0$) case has been studied by means of an asymptotic analysis and numerical Floquet Theory [8,10]. The presence of a countably infinite number of resonances within a finite range of parameter values makes this analysis problematic. It is well known that the inclusion of damping in the model not only makes the model more realistic, but also eliminates higher order resonances by shifting them to higher values of ε.

Fig. 5 shows the number of Floquet multipliers of the trivial solution outside the unit circle as a function of the frequency for $\varepsilon = 0.02$, a fixed value of B slightly below $B_{cr}^{(N)}$, for $N = 8$ and 16, and several values of the damping coefficient Γ.

The stability of the upright position is indicated by zero unstable multipliers, and jumps in the plot, which must be integer valued, corresponding to certain modes of instability. The undamped case (upper panel) shows a rich structure with many narrow windows of stability, interspersed with short peaks and plateau corresponding to the crossing of instability tongues. Clearly for $N = 16$ there is a more rapid variation, because of the greater number of spatial modes and hence greater propensity for parametric instability. Taking the limit $N \to \infty$ one would see an infinite number of such jumps (given infinite resolution) due to countably many resonances for a finite range of ω. Higher values of Γ broaden the regions of stability and decrease the number of narrow instabilities. This is in keeping with the idea that damping destroys narrow resonance tongues (more precisely moves them up to higher values of ε in a parameter plane); see for example Ref. [18]. Note too the similarity in the broad features of these instability plots for $N = 8$ and 16,
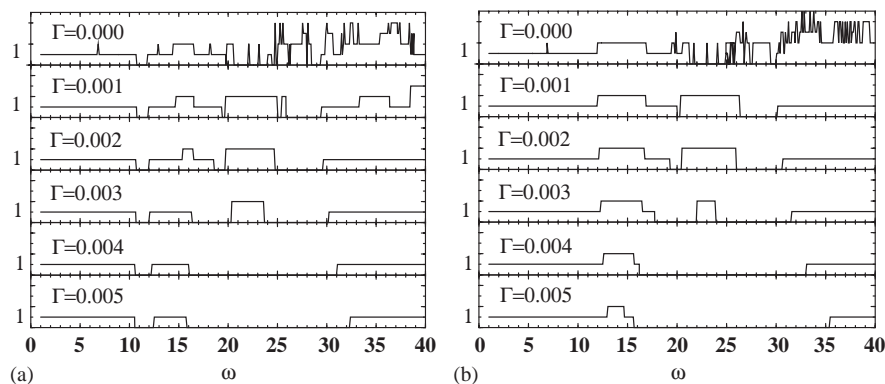

Fig. 5. Number of characteristic multipliers outside the unit circle as a function of ω for $N = 8$ (left) and $N = 16$ (right) for B-values slightly below the critical value ($B = 0.1814$ and $B = 0.1529$, respectively) and different values of the damping coefficient (Γ). The undamped case ($\Gamma = 0$) shows a rich structure with narrow and numerous windows of stability, whereas for higher values of Γ there are just broader windows of stability.

which indicates that only instabilities corresponding to simple (i.e., few noded) spatial modes will survive as damping is increased for fixed amplitude ε. For the rest of the paper the damping coefficient will be fixed at $\Gamma = 0.004$, and the effect of the remaining parameters will be studied. In practice, it is hard to measure material damping of a continuous structure accurately, but this particular Γ-value is chosen as it keeps just 2 or 3 instabilities within the ω-range that is used in Mullin's experiment.

4.4. The stiffness–amplitude bifurcation diagram

In Section 3.1 it was shown that the B–ε bifurcation diagram for the single pendulum coincides with the classical result for the Mathieu equation. This picture becomes more complicated as the number of pendulums increases. In Fig. 6 the same bifurcation diagram is shown for $\Gamma = 0.004$ and $N = 8$ and two values of the frequency; $\omega = 10$ and 20. The digits in the different regions denote the number of multipliers outside the unit circle. Each bifurcation curve has been labelled with the symbol BP, PD or TR according to the kind of bifurcation (branching point, period doubling or torus bifurcation, respectively), and the stability regions have been shaded. Note that the main effect of the damping is to lift the resonance tongues away from $\varepsilon = 0$. However, note that frequency ω also greatly affects the shape of the stability diagram. The two panels of Fig. 6 have some broad features the same and others that are quite different. The fundamental pitchfork bifurcation connecting to B_{cr} at $\varepsilon = 0$ behaves qualitatively the same. However, the ordering and shape of the other instabilities depends crucially on ω, just as it did for the undamped continuous model in Refs. [8,10]. This indicates that, unlike the case $N = 1$ where Section 3 showed that B and ω essentially play the same role in the linear problem, this is a genuine three-parameter problem (for fixed Γ).

4.5. The stiffness–frequency bifurcation diagram

The original motivation for the introduction of a model of N pendulums with elastic stiffness and damping, was to gain some understanding into the problem of stabilizing an elastic and
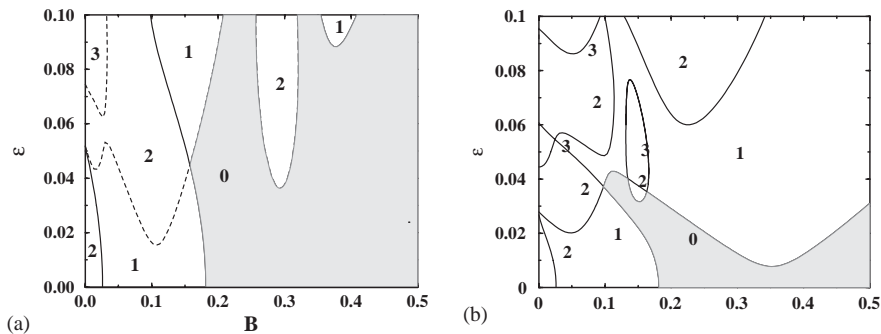

Fig. 6. Amplitude–elastic stiffness (B–ε) bifurcation diagram for $N = 8$, damping factor $\Gamma = 0.004$ and fixed frequency $\omega = 10$ (a) and $\omega = 20$ (b). The digits in the different regions denote the number of multipliers outside the unit circle. The solid lines correspond to pitchfork bifurcation (BP), the dotted lines to period doubling (PD), and the long dashed to torus bifurcation curves, respectively.
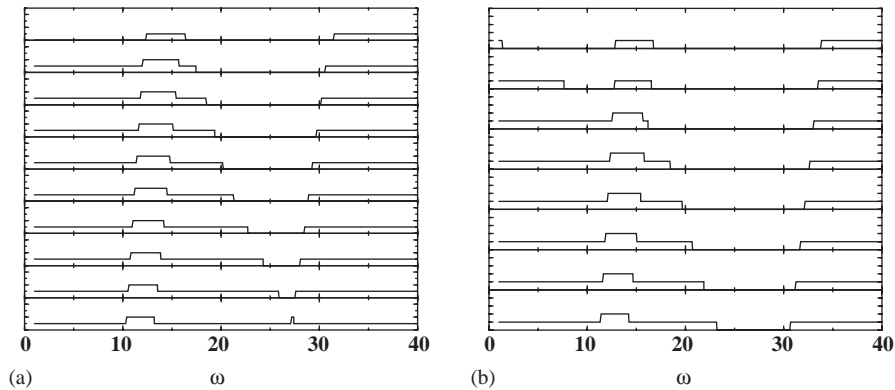
Fig. 7. Number of characteristic multipliers outside the unit circle for $N = 8$ (a) and $N = 16$ (b), $\Gamma = 0.004$ and decreasing values of B. The upper curves correspond to the critical value and the system of pendulums are stable even for vanishing frequencies. As the elastic component is lowered, the stability regions shrink. The small plateaus with 2 characteristic multipliers outside the unit circle reveal further bifurcations of the already unstable system.

damped curtain wire. By varying the length of the specimen of wire in order to vary the dimensionless parameter B, the most readily experimentally testable results are found by plotting results in the (B, ω)-parameter plane for fixed ε.

In order to see whether the stability results of the authors discrete model can be related to the continuum one, the number of characteristic multipliers outside the unit circle are plotted in Fig. 7 as the parameters ω and B are varied, for $N = 8$ (left) and $N = 16$ (right). The upper curve is the result for the *critical value of B* and the histograms below correspond to decreasing values of the elastic stiffness. Recall that if B is above the critical value the system is *stable* in its upright position, even without forcing. As the elastic component is lowered, the stability regions shrink. The small plateau with two characteristic multipliers outside the unit circle reveal further bifurcations of the already unstable system. These figures indicate that there is a qualitative agreement with the experimental results.

Fig. 8 is the main result of this paper. It is the (B, ω)-bifurcation diagram for fixed $\varepsilon = 0.02$, $\Gamma = 0.04$, $N = 8$ (left) and $N = 16$ (right). There are two stability regions (shaded) that are limited by curves of pitchfork (BP) and period doubling bifurcations (PD). The window at lower frequency is small and only exits close to the critical value of B. The digits inside each region denote the number of multipliers outside the unit circle.

In Fig. 9 is plotted a schematic representation of the mode that becomes unstable, by taking snapshots at given instants of time, at a characteristic point along each of the curves marked by BP, PD1 and PD2 in Fig. 8. Plotting the linear mode shape represents small amplitude motion near each instability, and normalizes the solutions by forcing the sum of the maximum of the components to be one. For ease of illustration it has been chosen to plot these modes for $N = 8$; mode shapes for $N = 16$ are found to be qualitatively the same.

Note that natural experimentally controllable parameters are the driving frequency and the total length of the wire. In the dimensionless equation, these broadly speaking refer to varying B and ω, but since the length of the wire also affects ε, one must also vary the time scale, the dimensionless driving amplitude, the elastic term and the effective damping factor in the
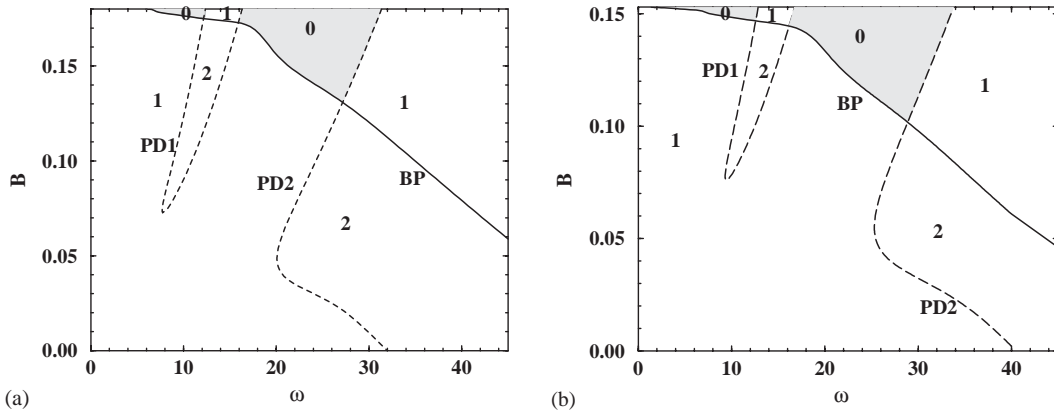
Fig. 8. *B–ω* bifurcation set for fixed *ε* = 0.02, *Γ* = 0.004, *N* = 8 (left) and *N* = 16 (right). The digits inside each regions denote the number of multipliers outside the unit circle. The stable regions have been shaded and are limited by curves of pitchfork (BP) and period doubling bifurcations (PD). A schematic representation of the mode that becomes unstable is also included at several points in the diagram.
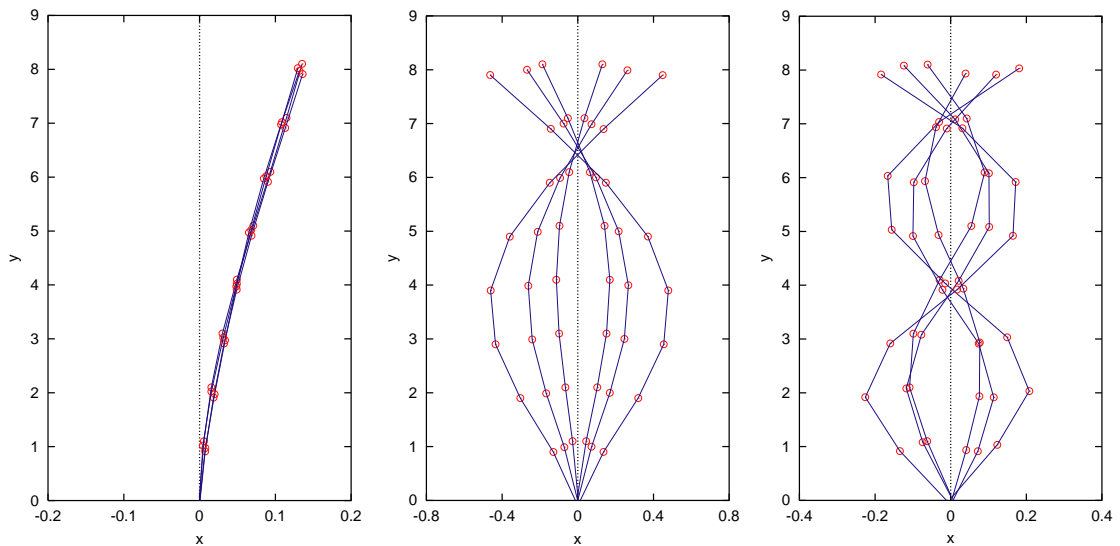

Fig. 9. Representation of the modes that become unstable for *N* = 8 pendulums when crossing the borders in the *B–ω* bifurcation diagram at the curves labeld by BP, PD1 and PD2, respectively. Snapshots of the multiple pendulums are shown at different instants of time within a period.

dimensionless model. A careful comparison with the experiments and such a process will be written up elsewhere [9]. At this stage though it is worth mentioning that the broad shape of the stability region in Fig. 8 corresponds to that of the experiments. The mode shape of the BP instability corresponds to what is observed in the experiment too as does that of the PD2 curve that bounds the main stability curve. The one caveat is that in the experiments and in the theory of Ref. [10], this mode shape is at harmonic resonance with the drive frequency rather than at subharmonic as here.

5. Conclusions

This paper demonstrates that a multiple linked pendulum model with bending stiffness and damping can be made stable in the upside down configuration by parametric resonance. Moreover by correctly scaling it has been demonstrated how this model approaches that of a continuously flexible rod with the inclusion of realistic material damping. This then leads to an effective way of performing numerical stability analysis on the continuum problem for which the inclusion of damping precludes a straightforward asymptotic analysis. Indeed these results show that damping has the effect of removing all but the few simplest instabilities for a fixed amplitude of parametric excitation. Moreover, these instabilities are well captured by an N-linked model with small N. The shape of the instability curves and the mode shapes of the corresponding instabilities well matched to those of an experiment on curtain wire, with one caveat. In broad terms it has been shown that the phenomenon of stabilization of rods by parametric excitation shown in Refs. [8,10] is robust under the inclusion of damping. The full non-linear dynamics of the N-linked model remain to be investigated. Taking the case $N = 1$, it has been shown how non-linear effects lead to hysteresis and have also related what is observed to known results for the simple pendulum (with dimensionless bending stiffness $B = 0$). The authors have also argued how the inclusion of small bending stiffness in the support has a stabilizing influence, whereas large B can paradoxically lead to instability. Presumably, the non-linear dynamics of the N-linked model will be far richer.

Acknowledgements

References

[1] A. Stephenson, On a new type of dynamical stability, *Memoirs and Proceedings of the Manchester Literary and Philosophical Society* 52 (1908) 1–10.
[2] D.J. Acheson, A pendulum theorem, *Proceedings of the Royal Society of London A* 443 (1993) 239–245.
[3] S. Otterbein, Stabilisierung des n-Pendels und der Indische Seiltrick, *Archive for Rational Mechanics and Analysis* 78 (1982) 381–393.
[4] D.J. Acheson, T. Mullin, Upside-down pendulums, *Nature* London 366 (1993) 215–216.
[5] C.A. Hurst, The Indian rope trick explained, *Australian Mathematical Society Gazette* 23 (1996) 154–159.
[6] D.J. Acheson, T. Mullin, Ropy magic, *New Scientist* 157 (1998) 32–33.
[7] D.J. Acheson, *From Calculus to Chaos, An Introduction to Dynamics*, Oxford University Press, Oxford, 1997.
[8] A.R. Champneys, W.B. Fraser, The 'Indian rope trick' for a parametrically excited rod: linearized analysis, *Proceedings of the Royal Society of London* 456 (2000) 553–570.
[9] T. Mullin, A.R. Champneys, B.W. Fraser, J. Galán, D. Acheson, The 'Indian wire trick' via parametric excitation: a comparison between theory and experiment, *Proceedings of the Royal Society London A* 459 (2003) 539–546.

[10] B.W. Fraser, A.R. Champneys, The 'Indian rope trick' for a parametrically excited rod; nonlinear and subharmonic analysis, *Proceedings of the Royal Society of London A* 458 (2002) 1353–1373.

[11] V.I. Arnold, *Ordinary Differential Equations*, MIT Press, Cambridge, MA, 1973.

[12] D.W. Jordan, P. Smith, *Nonlinear Ordinary Differential Equations*, 2nd Edition, Clarendon Press, Oxford, 1987.

[13] C. Chicone, *Ordinary Differential Equations with Applications*, Springer, New York, 1999.

[14] M. van Noort, The Parametrically Forced Pendulum, Ph.D. Thesis, University of Groningen, 2001.

[15] M. Levi, Geometry and physics of averaging with applications, *Physica D* 132 (1999) 150–164.

[16] E.J. Doedel, A.R. Champneys, T.F. Fairgrieve, Yu.A. Kuznetsov, B. Sandstede, X.J. Wang, *AUTO97: software for continuation and bifurcation problems in ordinary differential equations*, Department of Computer Science, Concordia University, Montreal, Canada, 1997. (`sourceforge.net/projects/auto2000`).

[17] A.G. Greenhill, Determination of the greatest height consistent with stability that a pole or mast can be made… ., *Proceedings of the Cambridge Philosophical Society* IV (1881) 65–73.

[18] A.H. Nayfey, D.T. Mook, *Nonlinear Oscillations*, Wiley Interscience, New York, 1970.